Available online at www.sciencedirect.com
SCIENCE DIRECT®
ELSEVIER
Journal of Computational and Applied Mathematics 168 (2004) 191–205
JOURNAL OF COMPUTATIONAL AND APPLIED MATHEMATICS
www.elsevier.com/locate/cam

Coupling scalar and vector potentials on nonmatching grids for eddy currents in a moving conductor

B. Flemisch[a], Y. Maday[b], F. Rapetti[c,*], B.I. Wohlmuth[a]

[a] *Inst. Ang. Analysis und Numer. Simulation, Univ. Stuttgart, Pfaffenwaldring 57, Stuttgart 70569, Germany*
[b] *Lab. J.-L. Lions, CNRS & Université de Paris VI, 4 place Jussieu, Paris 05 75252, France*
[c] *Lab. J.-A. Dieudonné, CNRS & Université de Nice, Parc Valrose, Nice 02 F-06108, France*

Received 27 September 2002; received in revised form 12 May 2003

Abstract

The $T-\Omega$ formulation of the magnetic field has been introduced in many papers for the approximation of the magnetic quantities modelled by the eddy current equations. This decomposition allows to use a scalar function in the main part of the computational domain, reducing the use of vector quantities to the conducting parts. We propose to approximate these two quantities on nonmatching grids so as to be able to tackle a problem where the conducting part can move in the global domain. The connection between the two grids is managed with mortar element techniques.
© 2003 Elsevier B.V. All rights reserved.

MSC: 78A30; 35Q60; 65N30; 65M55; 68U20

Keywords: Eddy currents; Scalar and vector potentials; Nonmatching grids; Domain decomposition; Mortar element methods

1. Problem setting

Low frequency electromagnetic devices are often modelled numerically on the basis of the eddy current formulation [1]. Two main families of formulations are widely used, the one based on magnetic and the one based on electric fields. In this paper, we restrict ourselves to the magnetic field approach. The space $\mathbb{R}^3$ is decomposed in the conducting region V_c and the external region $\mathbb{R}^3\backslash V_c$. Denoting by H, B, J and E the magnetic field, the magnetic flux density, the current density

* Corresponding author.
E-mail address: frapetti@math1.unice.fr (F. Rapetti).

0377-0427/$ - see front matter © 2003 Elsevier B.V. All rights reserved.
doi:10.1016/j.cam.2003.05.017

and the electric field, respectively, the quasi-stationary Maxwell equations restricted to the conducting region V_c read as follows:

$$\nabla \times H = J, \quad \nabla \times E = -\partial_t B, \quad \nabla \cdot B = 0. \tag{1}$$

The densities and the fields are linked by the constitutive properties, i.e., $B = \mu H$, $J = \sigma E$, where $\mu = \mu_0 \mu_r > 0$ is the magnetic permeability (the symbol μ_0 denotes the magnetic permeability of the air while $\mu_r > 1$ is the relative permeability of the medium) and $\sigma > 0$ stands for the electric conductivity. Moreover, we assume that the material parameters are time independent and associated with linear isotropic media, and that the external source J_s is zero within the conducting regions. As a result, we obtain the following field equations in $\mathbb{R}^3 \backslash V_c$:

$$\nabla \times H = J_s, \quad \nabla \cdot B = 0, \quad B = \mu H. \tag{2}$$

The problem is well posed by adding regularity conditions at infinity and suitable interface conditions on ∂V_c. In particular, $[H]_c \times n_c = 0$, $[B]_c \cdot n_c = 0$, $E \times n_c = 0$ and $J \cdot n_c = 0$, where n_c is the outer normal on ∂V_c, and $[v]_c$ stands for the jump of v on ∂V_c. These interface conditions have also to be verified at any surface where σ or μ is discontinuous. Additionally to the boundary conditions, we have to impose suitable initial values for the vector fields at a given time t_0. In particular, the initial condition on B has to satisfy $\nabla \cdot B = 0$ and $[B] \cdot n = 0$ at any interface. The condition $\nabla \cdot B = 0$ is satisfied at any time provided that it is verified by the initial condition. We point out the fact that the vector fields J and $\partial_t B$ are automatically forced to be solenoidal by (1). By introducing artificial boundary conditions, we can work on a bounded domain V. Furthermore, we assume that V_c is a simply connected polyhedral subdomain of V and $\bar{V}_c \subset V$.

For simplicity, in all the following integral equations, we omit the infinitesimal element of integration. In a weak form, $\nabla \cdot B = 0$ and $B = \mu H$ read as follows:

$$\int_V \mu H \nabla v = 0, \quad \forall v \in H_0^1(V), \tag{3}$$

where $H_0^1(V) = \{v \in L^2(V) \mid \nabla v \in L^2(V)^3,\ v_{|\partial V} = 0\}$. In terms of (1), we can write

$$\int_{V_c} \nabla \times H \nabla \times W + \int_{V_c} \sigma \partial_t(\mu H) W = 0, \quad \forall W \in H_0(\mathrm{curl}; V_c), \tag{4}$$

where $H_0(\mathrm{curl}; V_c) = \{W \in L^2(V_c)^3 \mid \nabla \times W \in L^2(V_c)^3, (W \times n_c)_{|\partial V_c} = 0\}$. For the current density J, the condition $\nabla \cdot J = 0$ suggests the introduction of a vector potential $\tilde{T}$ such that $J = \nabla \times \tilde{T}$. Then in V_c, the difference between the vector potential $\tilde{T}$ and the magnetic field H can be written as the gradient of a scalar function $\tilde{\Omega}$, i.e., $H = \tilde{T} - \nabla \tilde{\Omega}$. A similar argument holds for the insulating region, where we assume knowing a vector potential T_s such that $J_s = \nabla \times T_s$. Combining external and conducting regions, we write H as $H = \tilde{T} - \nabla \tilde{\Omega}$ in V_c and $H = T_s - \nabla \tilde{\Omega}$ in $V \backslash V_c$.

By eliminating the magnetic field H in (3) and (4), we obtain a coupled eddy current problem in terms of the vector potential $\tilde{T}$ defined only in the conducting region V_c and the scalar potential $\tilde{\Omega}$ defined everywhere in V. This system is completed with appropriate interface conditions on ∂V_c stating, e.g., that $\tilde{\Omega}$ is continuous. This is nevertheless not enough to define $\tilde{\Omega}$ and $\tilde{T}$ uniquely.

In fact $\nabla \cdot \tilde{T}$ is not specified, and thus there are many different gauge possibilities. One of them is to require that $\tilde{T}$ has the same divergence as H in V_c but this eliminates $\tilde{\Omega}$ on V_c. We prefer another condition, given in Section 2.

Remark 1. In the considered configuration, the conductor V_c can freely move in V. In presence of moving conductors, we have to choose the reference system with respect to which we write the eddy current problem. Let $\mathscr{R}$ be a reference system linked to V and $\mathscr{R}_c$ be a reference system linked to V_c. If v is the conductor velocity, the appropriate form of Ohm's law in the reference system $\mathscr{R}$ reads

$$J = \sigma(E + v \times B) \quad \text{in } V_c \quad \text{and} \quad J = \sigma E \quad \text{in } V.$$

The motion of V_c is directly considered in the convective term $v \times B$. This is a typical feature of the Eulerian description, i.e., the use of a single reference system for both parts V and V_c. To get rid of the explicit velocity term, it is advisable to use as many different frames as the number of parts, that is, in our case, to reformulate with respect to $\mathscr{R}$ the equations in V and with respect to $\mathscr{R}_c$ the equations in V_c. This is the Lagrangian description, where the spectator is attached to the considered part and describes the events from his material point of view. This approach makes disappear the explicit velocity term from Ohm's law, provided that each part is treated in its own "co-moving" frame ($\mathscr{R}$ with V and $\mathscr{R}_c$ co-moving with V_c). If two different reference systems are used, one has to couple both by suitable transmission conditions at the conductor boundary. We stress out the fact that for the analysis of eddy current problems in domains with moving parts, there is some freedom in the choice of the reference frame, provided that the motion can be regarded as quasi-stationary with respect to electro-dynamics. This freedom is a consequence of the low frequency limit. However, this is not possible for the full set of Maxwell's equations, where already a small acceleration can have a significant effect (see [4] and the references therein). Thanks to this characteristic of the eddy current model, we can adopt the "piecewise Lagrangian approach" (a Lagrangian approach on each part). This allows us to work with independent meshes and discretizations. To do so, we use mortar techniques realizing the coupling of scalar and vector potentials on nonmatching grids. This approach has been introduced in [7] and analyzed in [8]. Classical techniques often rely on the use of boundary elements [10], or on the fictitious domain approach [6].

2. Variational problem

In this section, we define a variational formulation based on the decomposition of H into $\tilde{T}$ and $\nabla\tilde{\Omega}$. We restrict ourselves to the system obtained after time discretization of (3) and (4). Using a stable implicit Euler scheme with time step δt, we have to face a variational problem at each time step: find $(\tilde{T}, \tilde{\Omega}) \in H_0(\mathrm{curl}; V_c) \times H_0^1(V)$ such that

$$\begin{aligned} a(\tilde{\Omega}, v) + \hat{b}_c(\tilde{T}, v) &= \int_{V \setminus V_c} f \nabla v, \quad \forall v \in H_0^1(V), \\ a_c(\tilde{T}, W) + \hat{b}_c(W, \tilde{\Omega}) &= \int_{V_c} f_c W, \quad \forall W \in H_0(\mathrm{curl}; V_c). \end{aligned} \tag{5}$$

Here, the continuous bilinear forms are defined by

$$\hat{b}_c(W,v) = -\int_{V_c} W\nabla v, \quad \forall W \in H_0(\mathrm{curl}; V_c),\ \forall v \in H_0^1(V),$$

$$a(\tilde{\Omega}, v) = \int_V \beta\nabla\tilde{\Omega}\nabla v, \quad \forall\tilde{\Omega},\ v \in H_0^1(V),$$

$$a_c(\tilde{T}, W) = \int_{V_c} (\alpha\nabla\times\tilde{T}\nabla\times W + \tilde{T}W), \quad \forall\tilde{T},\ W \in H_0(\mathrm{curl}, V_c),$$

where the coefficients $\alpha, \beta > 0$ are assumed to be piecewise constant. In the more general approach, they are uniformly positive definite and depend on the material parameters σ, μ as well as on the time step (e.g., $\alpha = \delta t/\mu\sigma$ in V_c). Note that the unknowns $\tilde{T}$ and $\tilde{\Omega}$ denote the approximations at the current time step, f_c depends on the approximations of $\tilde{T}$ and $\tilde{\Omega}$ at the previous time step, and f denotes the scaled source term depending on T_s. Choosing $\tilde{T} \in H_0(\mathrm{curl}; V_c)$ and $\tilde{\Omega} \in H_0^1(V)$, $\tilde{T}$ and $\tilde{\Omega}$ satisfy at each time step the interface conditions, i.e., $\tilde{\Omega}$ is continuous at ∂V_c and $[T]_c \times n_c = 0$.

In our approach, the strong coupling between $\tilde{T}$ and $\tilde{\Omega}$ at the interface is replaced by a weak one.

It is easy to see that if $(\tilde{T}, \tilde{\Omega})$ is a solution of (5), then $(\tilde{T} + \nabla\phi, \tilde{\Omega} + \phi)$, $\phi \in H_0^1(V_c)$, is a solution as well. In order to get uniqueness, we choose ϕ such that $\Omega = \tilde{\Omega} + \phi$ is harmonic on V_c. We introduce the harmonic extension operator $\mathscr{H} : H^{1/2}(\partial V_c) \to H^1(V_c)$ satisfying

$$(\mathscr{H}v)_{|\partial V_c} = v, \quad \int_{V_c} \nabla\mathscr{H}v\nabla w = 0, \quad \forall w \in H_0^1(V_c), \tag{6}$$

and state the modified variational problem: find $(T, \Omega) \in H_0(\mathrm{curl}; V_c) \times H_0^1(V)$ such that

$$a(\Omega, v) + b_c(T, v) = \int_{V\setminus V_c} f\nabla v, \quad \forall v \in H_0^1(V),$$

$$a_c(T, W) + b_c(W, \Omega) = \int_{V_c} f_c W, \quad \forall W \in H_0(\mathrm{curl}; V_c), \tag{7}$$

where $b_c(W, v) = -\int_{V_c} W\nabla\mathscr{H}v_{|\partial V_c}$, for $v \in H_0^1(V)$ and $W \in H_0(\mathrm{curl}; V_c)$. The bilinear form given by

$$a_g((W, w), (V, v)) = a_c(W, V) + b_c(W, v) + b_c(V, w) + a(w, v),$$

where $V, W \in H_0(\mathrm{curl}; V_c)$ and $v, w \in H_0^1(V)$, is elliptic on $H_0(\mathrm{curl}; V_c) \times H_0^1(V)$; see [8]. Consequently, the variational problem (7) has a unique solution. The first equation in (7) and the definition of the harmonic extension yield $b_c(T, v) = 0$, $\forall v \in H_0^1(V_c)$. Using $W = \nabla v$, $v \in H_0^1(V_c)$, in the second equation of (7), we find that T is divergence free if f_c is divergence free. Hence, T is implicitly gauged, and Ω restricted to V_c is harmonic.

3. Discretization

We use two different quasi-uniform triangulations $\mathfrak{T}_H$ on V and $\mathfrak{T}_h$ on V_c. Here, H and h denote the maximal diameter of the elements of the triangulation $\mathfrak{T}_H$ and $\mathfrak{T}_h$, respectively. On $\mathfrak{T}_H$, we use standard conforming finite elements of lowest order for the approximation of the scalar potential Ω. The associated discrete space having zero boundary conditions on ∂V is called $S_{0;H}(V)$. For the

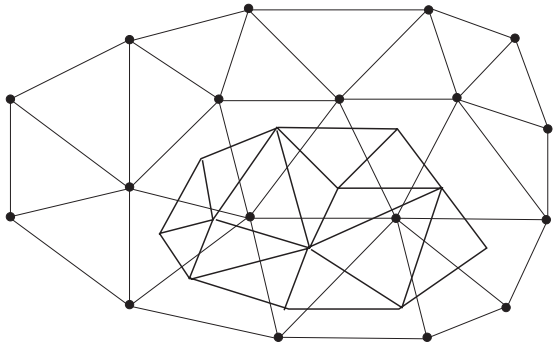

Fig. 1. Overlapping decomposition and nonmatching triangulations on V_c in two-dimensions.

discretization of the vector field T, we use lowest order curl-conforming Nédélec finite elements on $\mathfrak{T}_h$. The basis functions w_e are associated with the edges e of the triangulation $\mathfrak{T}_h$ and are also known as edge elements [9]. They can be defined in terms of the standard H^1-conforming nodal basis functions φ_p by

$$w_e = \varphi_p \nabla \varphi_q - \varphi_q \nabla \varphi_p,$$

where the edge $e = \{p, q\}$ is oriented from node p to node q. The orientation of the edges can be chosen arbitrarily. We set $X_h(V_c) = \text{span}\{w_e \mid e \text{ edge} \in \mathfrak{T}_h\}$ and $X_{0;h}(V_c) = X_h(V_c) \cap H_0(\text{curl}; V_c)$. Note that the elements $T \in X_{0;h}(V_c)$ have vanishing tangential components on ∂V_c. Finally, we denote by $S_h(V_c)$ the space of standard conforming finite elements of lowest order associated with $\mathfrak{T}_h$ on V_c, and its trace space on ∂V_c is called $W_h(\partial V_c)$. We remark that no boundary conditions are imposed on $S_h(V_c)$.

Fig. 1 illustrates the situation in two-dimensions. In general, the triangulations $\mathfrak{T}_h$ and $\mathfrak{T}_H$ do not coincide on V_c, i.e., the two triangulations are nonmatching. Moreover, the subdomain V_c cannot be written as the union of elements in $\mathfrak{T}_H$.

In order to formulate the discrete version of the variational problem (7), we have to replace the harmonic extension (6) in the definition of the bilinear form $b_c(\cdot, \cdot)$. A natural choice is to involve the discrete harmonic extension $\mathscr{H}_h$ defined as a map $\mathscr{H}_h : \mathbb{W}_h(\partial V_c) \to S_h(V_c)$ verifying

$$(\mathscr{H}_h v)_{|_{\partial V_c}} = v, \quad \int_{V_c} \nabla \mathscr{H}_h v \nabla w = 0, \quad \forall w \in S_h(V_c) \cap H_0^1(V_c).$$

The restriction of $v \in S_{0;H}(V)$ on ∂V_c is, in general, not an element in $\mathbb{W}_h(\partial V_c)$. Thus, we cannot apply directly the discrete harmonic extension to the restriction of $v \in S_{0;H}(V)$ on ∂V_c. To overcome this difficulty, we introduce a projection operator Π_h on the boundary ∂V_c. This operator is well known in the mortar finite element context [2] and can be defined in terms of a Lagrange multiplier space $\mathbb{M}_h(\partial V_c)$:

$$\Pi_h : H^1(V) \to \mathbb{W}_h(\partial V_c), \quad \int_{\partial V_c} \Pi_h v v = \int_{\partial V_c} v v, \quad \forall v \in \mathbb{M}_h(\partial V_c). \tag{8}$$

Note that the choice of the projection operator Π_h is important in order to build efficient algorithms of optimal complexity. Moreover, to obtain a well defined operator Π_h, the Lagrange multiplier

space $\mathbb{M}_h(\partial V_c)$ has to be chosen properly. There are many possibilities, but for simplicity reasons, we restrict ourselves to two choices. In the first case, we use the trace space and set $\mathbb{M}_h(\partial V_c)=\mathbb{W}_h(\partial V_c)$, see [2]. Then, the operator Π_h is a L^2-projection, and a mass matrix system has to be solved. In the second case, we replace the trace space by a so-called dual Lagrange multiplier space, see [12]. Then, Π_h is a quasi L^2-projection having the same qualitative stability properties as before. The advantage is that the mass matrix system is diagonal. Both choices guarantee that the operator Π_h is H^s-stable for $0 \leqslant s \leqslant 1$. Furthermore, it satisfies the approximation property in the $H^{1/2}$-norm and in the $H^{-1/2}$-norm. In terms of the operators $\mathscr{H}_h$ and Π_h, we formulate the new discrete variational problem: find $(T_h, \Omega_H) \in X_{0;h}(V_c) \times S_{0;H}(V)$ such that

$$a(\Omega_H, v) + b_h(T_h, v) = \int_{V \setminus V_c} f \nabla v, \quad \forall v \in S_{0;H}(V),$$

$$a_c(T_h, W) + b_h(W, \Omega_H) = \int_{V_c} f_c W, \quad \forall W \in X_{0;h}(V_c), \tag{9}$$

where $b_h(W, v) = -\int_{V_c} W \nabla \mathscr{H}_h \Pi_h v$, for $v \in S_{0;H}(V)$ and $W \in X_{0;h}(V_c)$. This approach is characterized by an optimal error estimate, as stated in the next lemma which is proved in [8].

Lemma 2. *For h/H small enough, the discrete variational problem* (9) *has a unique solution and there exists a constant C independent of the meshsize such that, for $T \in H^1(V_c)^3$ with $\nabla \times T \in H^1(V_c)^3$ and $\Omega \in H^\beta(V)$, $1 < \beta \leqslant 2$, we have*

$$|||T - T_h|||_{V_c} + \|\Omega - \Omega_H\|_{1;V} \leqslant C(h(\|T\|_{1;V_c} + \|\nabla \times T\|_{1;V_c}) + H^{\beta-1}\|\Omega\|_{\beta;V}),$$

where $|||T|||_{V_c} = (\|T\|^2_{0;V_c} + \alpha\|\nabla \times T\|^2_{0;V_c})^{1/2}$ is a norm which is equivalent to the standard Hilbert space norm on $H_0(\mathrm{curl}; V_c)$.

4. Implementation and algorithmic details

In this section, we focus our attention on the numerical realization of the scalar and vector potentials' coupling. The first and most delicate step of this coupling is the definition of the values of $v_H \in S_{0;H}(V)$ at the nodes of $\mathfrak{T}_h$ which belong to ∂V_c. For this purpose, we involve the mortar element projection operator Π_h defined in (8). From now on, we denote by $\Gamma = \partial V_c$ the surface on which the mortar projection is defined. The value $v^- = \Pi_h v_H \in \mathbb{W}_h(\Gamma)$ is called *non-mortar* (slave) value of the *mortar* (master) value $v^+ = v_{H|_\Gamma}$. Starting with an element $v_H \in S_{0;H}(V)$, we have to compute $\Pi_h v_H$. Let $\mathfrak{V}_h^-$, $\mathfrak{E}_h$ and $\mathfrak{V}_H^+$ denote the set of all nodes of the non-mortar mesh $\mathfrak{T}_h$ lying on Γ, the set of all boundary faces of $\mathfrak{T}_h$, and the set of all nodes of the mortar mesh $\mathfrak{T}_H$ belonging to a tetrahedron that intersects a face of $\mathfrak{E}_h$, respectively.

According to Fig. 2 (a two-dimensional example, where the words "face" and "tetrahedron" have to be replaced by "edge" and "triangle", respectively), we have

$$\mathfrak{E}_h = \{\mathrm{I}, \mathrm{II}, \mathrm{III}\}, \quad \mathfrak{V}_h^- = \{\boxed{1}, \boxed{2}, \boxed{3}, \boxed{4}\}, \quad \mathfrak{V}_H^+ = \{1, 2, 3, 4, 5, 7, 8, 9, 10\}.$$

The computation of $q_{\ell k}^- = \int_\Gamma \varphi_k^- \psi_\ell^-$, where φ_k^- and ψ_ℓ^- are basis functions of $\mathbb{W}_h(\Gamma)$ and $\mathbb{M}_h(\Gamma)$, respectively, can easily be carried out. We note that both basis functions are defined with respect to

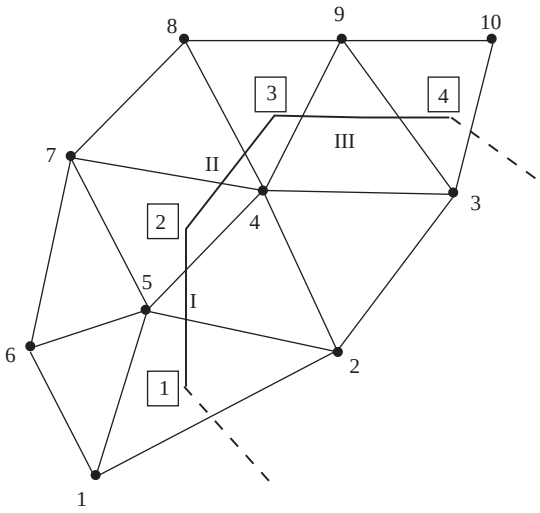

Fig. 2. Notations for the mortar element projection operator on Γ in two-dimensions.

the same mesh. On the contrary, the computation of $\int_\Gamma \varphi_k^+ \psi_\ell^-$, where φ_k^+ and ψ_ℓ^- are basis functions of $S_{0;H}(V)$ and $\mathbb{M}_h(\Gamma)$, respectively, involves discrete functions that live on different meshes. Fig. 2 illustrates the situation in two dimensions. To compute $\int_\Gamma \varphi_k^+ \psi_\ell^-$, we have to intersect the three-dimensional support of φ_k^+ on V with the two-dimensional one of ψ_ℓ^- on Γ. The exact computation of this intersection area is feasible in two dimensions but difficult in three-dimensional situations. Using quadrature formulas to evaluate $\int_\Gamma \varphi_k^+ \psi_\ell^-$ increases considerably the efficiency of the implementation and can be done as follows:

(i) we define a quadrature formula (ω_i^j, x_i^j), $1 \leqslant j \leqslant N_q$, on the face $s_i \in \mathfrak{E}_h$ by transforming a chosen quadrature formula defined on a reference face;
(ii) we localize each quadrature node x_i^j within $\mathfrak{T}_H$: we call $x_{i,H}^j$ the node position and note that x_i^j and $x_{i,H}^j$ coincide geometrically.
(iii) We then replace $\int_\Gamma \varphi_k^+ \psi_\ell^-$ by $q_{\ell k}^+ = \sum_{s_i \in \mathfrak{P}_\ell} \sum_{j=1}^{N_q} \omega_i^j \varphi_k^+(x_{i,H}^j) \psi_\ell^-(x_i^j)$, where $\mathfrak{P}_\ell$ is the set of faces in $\mathfrak{E}_h$ being in the support of ψ_ℓ^-.

In what follows, we use the same notation for the discrete functions and their algebraic representations with respect to the specified basis functions. The condition (8) can be now written in matrix form as $Q_- v^- = Q_+ v_H$, where $Q_- = (q_{\ell k}^-)_{\ell k}$ and $Q_+ = (q_{\ell k}^+)_{\ell k}$ are mass matrices. The nodes in $\mathfrak{T}_H$ being not in $\mathfrak{V}_H^+$ result in a zero column in Q_+ and do not have to be computed. As usual in the finite element context, the mass matrices Q_- and Q_+ can be assembled locally. Denoting by Q the rectangular product matrix $Q_-^{-1} Q_+$, the condition (8) reads $v^- = Q v_H$. Due to the reduced number of mesh nodes in $\mathfrak{V}_h^-$ the inversion of Q_- is not at all expensive compared to the global algorithm. Moreover, the matrix Q_- is diagonal in the case of a dual Lagrange multiplier space.

The second step of the coupling is the definition of the discrete harmonic extension $\mathscr{H}_h v^-$. This corresponds to solve a Dirichlet boundary problem in V_c for the Laplace operator with a zero source

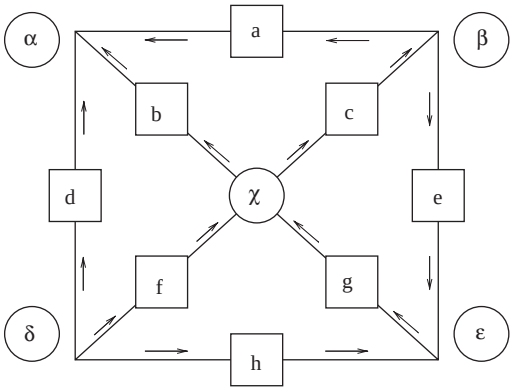

Fig. 3. Computing the node-to-edge incident matrix G in two-dimensions.

term and given boundary data on Γ. We denote by S the matrix associated with the harmonic extension $\mathscr{H}_h$ from $\mathbb{W}_h(\Gamma)$ to $S_h(V_c)$. Finally, we have to realize the coupling between the global scalar potential and the local vector one. We remark that the values of $W_h \in X_{0;h}(V_c)$ on the boundary edges are zero due to the homogeneous boundary condition on Γ. As it is classical, the vector $\nabla \mathscr{H}_h v^-$ can be decomposed in terms of the same edge element basis as W_h; the coefficients of the decomposition are circulations along the considered edges defined from nodal values at the end points of the edge. The passage from the nodal values to the associated circulation can be done efficiently by introducing the incidence matrix G, see also [3]. As we have seen, an edge is not only a two-node subset of the set of all mesh nodes, but an ordered subset where the order implies an orientation. Let $e = \{p, q\}$ be an edge of the mesh oriented from node p to node q. Then, we can define the incidence numbers $G(e,q) = 1$, $G(e,p) = -1$ and $G(e,r) = 0$ for all other nodes r. These numbers form a rectangular matrix G which describes how edges connect to nodes.

According to the example given in Fig. 3, where $\{\alpha, \beta, \delta, \chi, \varepsilon\}$ are the mesh nodes and $\{a, b, c, d, e, f, g, h\}$ the mesh edges, the node-to-edge operator is represented by the 8×5 matrix G that reads

$$G = \begin{pmatrix} 1 & -1 & 0 & 0 & 0 \\ 1 & 0 & 0 & -1 & 0 \\ 0 & 1 & 0 & -1 & 0 \\ 1 & 0 & -1 & 0 & 0 \\ 0 & -1 & 0 & 0 & 1 \\ 0 & 0 & -1 & 1 & 0 \\ 0 & 0 & 0 & 1 & -1 \\ 0 & 0 & -1 & 0 & 1 \end{pmatrix}.$$

Let $v \in S_h(V_c)$, then $W = \nabla v \in X_h(V_c)$. Using the node-to-edge incidence matrix G, the algebraic representation has the form $W = Gv$. Fig. 4 illustrates the action of the node-to-edge and edge-to-node operators G and G^t (the upper index t denotes the transposed operator).

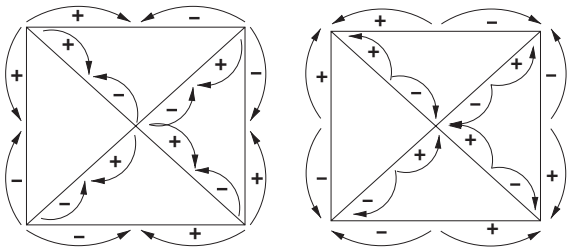

Fig. 4. The action of the node-to-edge and edge-to-node operators G and G^{t}.

We associate with $-\int_{V_c} W\nabla v$, $W \in X_h(V_c)$ and $v \in S_h(V_c)$, the rectangular matrix B. It can be written as $B = -MG$, where M is the edge element mass matrix on V_c. The stiffness matrix A associated with the bilinear form $a_c(\cdot,\cdot)$ on $X_h(V_c)\times X_h(V_c)$ can be decomposed in $A = M + C$ where C is associated with the curl part of $a_c(\cdot,\cdot)$, i.e., the elements of C are given by $(C)_{ee'} = \int_{V_c} \alpha\nabla \times w_e \nabla \times w_{e'}$, for all edges e, e' of $\mathfrak{T}_h$. Observing that $CG = 0$, due to the fact that curl(grad $\cdot$) $= 0$, we find $B = -AG$. If we now decompose the edges into boundary and interior edges, we can write A as a 2×2 block matrix

$$A = \begin{pmatrix} A_{\mathrm{II}} & A_{\mathrm{I}\Gamma} \\ A_{\Gamma\mathrm{I}} & A_{\Gamma\Gamma} \end{pmatrix} \quad \text{and} \quad A_0 = \begin{pmatrix} A_{\mathrm{II}} & A_{\mathrm{I}\Gamma} \\ 0 & \mathrm{Id} \end{pmatrix},$$

where A_0 is the matrix associated with the Dirichlet problem on $X_{0;h}(V_c)$ defined in terms of the same bilinear form $a_c(\cdot,\cdot)$.

We finally present a numerical algorithm to solve the discrete problem (9). Let us denote by $K_{0;V}$ the standard stiffness matrix associated with the bilinear form $a(\cdot,\cdot)$ on $H_0^1(V)\times H_0^1(V)$. The algebraic form of the discrete problem (9) reads: find two vectors T_h and Ω_H solving the linear system

$$A_0 T_h + PBSQ\Omega_H = F_c, \quad K_{0;V}\Omega_H + Q^{\mathrm{t}}S^{\mathrm{t}}B^{\mathrm{t}}T_h = F. \tag{10}$$

The right-hand side vectors take into account the homogeneous Dirichlet boundary conditions, and P is a cut off matrix; i.e., $P(v_I, v_\Gamma)^{\mathrm{t}} = (v_I, 0)^{\mathrm{t}}$. The application of P is necessary to guarantee the homogeneous Dirichlet boundary condition of T_h on Γ.

As iterative solver for (10), we propose a block Gauß–Seidel method. Starting from Ω_H^n, we first compute T_h^{n+1} and then Ω_H^{n+1} by

$$A_0 T_h^{n+1} + PBSQ\Omega_H^n = F_c, \quad K_{0;V}\Omega_H^{n+1} + Q^{\mathrm{t}}S^{\mathrm{t}}B^{\mathrm{t}}T_h^{n+1} = F. \tag{11}$$

The following lemma guarantees the convergence of the algorithm, see [8].

Lemma 3. *Let $e^n = \Omega_H - \Omega_H^n$ be the iteration error in the nth step, then there exists a constant $0 < \theta < 1$ not depending on H and h such that*

$$a(e^{n+1}, e^{n+1}) < \theta a(e^n, e^n).$$

The convergence of Ω_H^n to Ω_H yields the one of T_h^n to T_h.

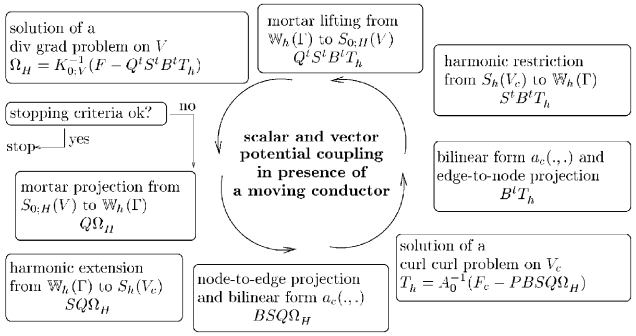

Fig. 5. Numerical algorithm for the scalar and vector potentials coupling.

Fig. 5 illustrates the algorithm. It is compatible with the presence of a conductor V_c that can move inside V. The construction of the mortar projection Π_h is the only part of the algorithm that is influenced by the motion of V_c. Thus, only the matrix Q has to be reassembled whenever the conductor V_c changes its position in V.

In the rest of this section, we present an equivalent formulation of (11). We denote by K the standard stiffness matrix associated with the Laplace operator on V_c corresponding to the bilinear form $\int_{V_c} \nabla v \nabla v'$.

Lemma 4. *The following identity holds*:

$$S^t B^t A_0^{-1} PBS = \mathscr{S}_K - G_{\Gamma\Gamma}^t \mathscr{S}_A G_{\Gamma\Gamma},$$

where $\mathscr{S}_A$ *and* $\mathscr{S}_K$ *is the Schur complement of* A *and* K, *respectively*, *i.e.*, $\mathscr{S}_A = A_{\Gamma\Gamma} - A_{\Gamma I} A_{II}^{-1} A_{I\Gamma}$.

Proof. We start by rewriting

$$\begin{aligned} AA_0^{-1}PA &= \begin{pmatrix} A_{II} & A_{I\Gamma} \\ A_{\Gamma I} & A_{\Gamma\Gamma} \end{pmatrix} \begin{pmatrix} A_{II}^{-1} & -A_{II}^{-1}A_{I\Gamma} \\ 0 & \mathrm{Id} \end{pmatrix} \begin{pmatrix} \mathrm{Id} & 0 \\ 0 & 0 \end{pmatrix} \begin{pmatrix} A_{II} & A_{I\Gamma} \\ A_{\Gamma I} & A_{\Gamma\Gamma} \end{pmatrix} \\ &= \begin{pmatrix} \mathrm{Id} & 0 \\ A_{\Gamma I}A_{II}^{-1} & \mathscr{S}_A \end{pmatrix} \begin{pmatrix} A_{II} & A_{I\Gamma} \\ 0 & 0 \end{pmatrix} = \begin{pmatrix} A_{II} & A_{I\Gamma} \\ A_{\Gamma I} & A_{\Gamma I}A_{II}^{-1}A_{I\Gamma} \end{pmatrix} \\ &= \begin{pmatrix} A_{II} & A_{I\Gamma} \\ A_{\Gamma I} & A_{\Gamma\Gamma} \end{pmatrix} - \begin{pmatrix} 0 & 0 \\ 0 & \mathscr{S}_A \end{pmatrix} = A - \begin{pmatrix} 0 & 0 \\ 0 & \mathscr{S}_A \end{pmatrix}. \end{aligned} \tag{12}$$

Recalling that $-B = AG = MG$ and thus $G^t AG = G^t MG = K$, we find

$$S^t G^t AGS = S^t KS = (-K_{\Gamma I}K_{II}^{-1}, \mathrm{Id}) \begin{pmatrix} K_{II} & K_{I\Gamma} \\ K_{\Gamma I} & K_{\Gamma\Gamma} \end{pmatrix} \begin{pmatrix} -K_{II}^{-1}K_{I\Gamma} \\ \mathrm{Id} \end{pmatrix} = \mathscr{S}_K.$$

Here, we have used a 2×2 block decomposition into interior and boundary vertices, and $\mathscr{S}_K$ stands for the Schur complement associated with K.

Finally, we have to consider the second term on the right-hand side of (12) in more detail. To do so, we use the block decomposition

$$G = \begin{pmatrix} G_{\mathrm{II}} & G_{\mathrm{I}\Gamma} \\ 0 & G_{\Gamma\Gamma} \end{pmatrix},$$

noting that $G_{\Gamma\mathrm{I}} = 0$ since an interior vertex cannot be an endpoint of an edge on the boundary. The block decomposition of G yields

$$S^{\mathrm{t}} G^{\mathrm{t}} \begin{pmatrix} 0 & 0 \\ 0 & \mathscr{S}_A \end{pmatrix} GS = (*, \mathrm{Id}) \begin{pmatrix} 0 & 0 \\ 0 & G_{\Gamma\Gamma}^{\mathrm{t}} \mathscr{S}_A G_{\Gamma\Gamma} \end{pmatrix} \begin{pmatrix} * \\ \mathrm{Id} \end{pmatrix} = G_{\Gamma\Gamma}^{\mathrm{t}} \mathscr{S}_A G_{\Gamma\Gamma}.$$

Summarizing the results, we find

$$S^{\mathrm{t}} B^{\mathrm{t}} A_0^{-1} PBS = S^{\mathrm{t}} G^{\mathrm{t}} A A_0^{-1} PAGS = \mathscr{S}_K - G_{\Gamma\Gamma}^{\mathrm{t}} \mathscr{S}_A G_{\Gamma\Gamma}. \qquad \square$$

Using the first equation in (10), we find $T_h = A_0^{-1}(F_{\mathrm{c}} - PBSQ\Omega_H)$. Then, the elimination of T_h in (10) and Lemma 4 yield a linear system for Ω_H:

$$(K_{0;V} - Q^{\mathrm{t}}(\mathscr{S}_K - G_{\Gamma\Gamma}^{\mathrm{t}} \mathscr{S}_A G_{\Gamma\Gamma})Q)\Omega_H = F - Q^{\mathrm{t}} S^{\mathrm{t}} B^{\mathrm{t}} A_0^{-1} F_{\mathrm{c}} = F_H. \tag{13}$$

If h/H is small enough, the matrix $K_{0;V} - Q^{\mathrm{t}}(\mathscr{S}_K - G_{\Gamma\Gamma}^{\mathrm{t}} \mathscr{S}_A G_{\Gamma\Gamma})Q$ is symmetric and positive definite, see [8]. Applying to (13) a Richardson iteration (see [11] for more details) with $K_{0;V}^{-1}$ as preconditioner yields

$$\begin{aligned} \Omega_H^{n+1} &= \Omega_H^n + K_{0;V}^{-1}(F_H - (K_{0;V} - Q^{\mathrm{t}}(\mathscr{S}_K - G_{\Gamma\Gamma}^{\mathrm{t}} \mathscr{S}_A G_{\Gamma\Gamma})Q)\Omega_H^n) \\ &= K_{0;V}^{-1}(F_H + Q^{\mathrm{t}}(\mathscr{S}_K - G_{\Gamma\Gamma}^{\mathrm{t}} \mathscr{S}_A G_{\Gamma\Gamma})Q\Omega_H^n). \end{aligned} \tag{14}$$

Lemma 5. *The block Gauß–Seidel method* (11) *with* $\Omega_H^0 = K_{0;V}^{-1} F_H$ *is equivalent to the preconditioned Richardson iteration* (14) *with the same* Ω_H^0.

Proof. The block Gauß–Seidel method yields the following recursive definition of T_h^{n+1}:

$$\begin{aligned} T_h^{n+1} &= A_0^{-1}(F_{\mathrm{c}} - PBSQ\Omega_H^n) = A_0^{-1}(F_{\mathrm{c}} - PBSQ\Omega_H^{n-1} + PBSQ(\Omega_H^{n-1} - \Omega_H^n)) \\ &= T_h^n - A_0^{-1} PBSQ(\Omega_H^n - \Omega_H^{n-1}), \end{aligned}$$

where we set $\Omega_H^{-1} = 0$ and $T_h^0 = A_0^{-1} F_{\mathrm{c}}$. Using $\Omega_H^0 = K_{0;V}^{-1} F_H$, we find for the block Gauß–Seidel method

$$\begin{aligned} K_{0;V}\Omega_H^{n+1} &= F - Q^{\mathrm{t}} S^{\mathrm{t}} B^{\mathrm{t}} T_h^n + Q^{\mathrm{t}} S^{\mathrm{t}} B^{\mathrm{t}} A_0^{-1} PBSQ(\Omega_H^n - \Omega_H^{n-1}) \\ \Omega_H^{n+1} &= \Omega_H^n + K_{0;V}^{-1} Q^{\mathrm{t}} S^{\mathrm{t}} B^{\mathrm{t}} A_0^{-1} PBSQ(\Omega_H^n - \Omega_H^{n-1}). \end{aligned}$$

By means of Lemma 4, we get that the Gauß–Seidel method (11) is equivalent to

$$\Omega_H^{n+1} = \Omega_H^n + K_{0;V}^{-1} Q^{\mathrm{t}}(\mathscr{S}_K - G_{\Gamma\Gamma}^{\mathrm{t}} \mathscr{S}_A G_{\Gamma\Gamma})Q(\Omega_H^n - \Omega_H^{n-1}). \tag{15}$$

Comparing (14) and (15), the assertion can be easily shown by induction. $\square$

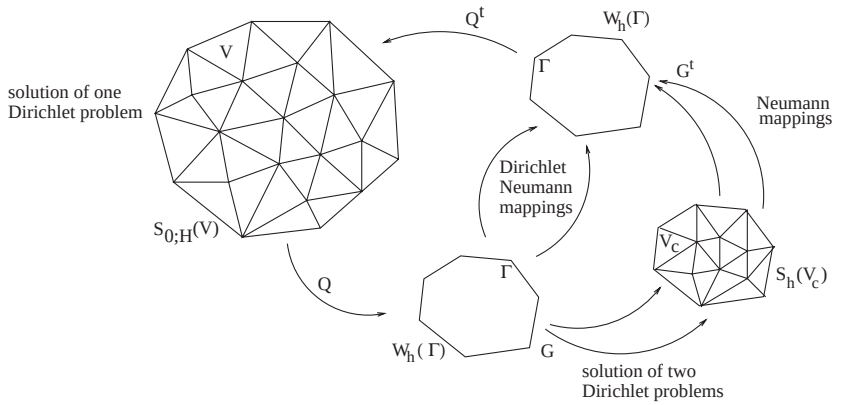

Fig. 6. Illustration of the preconditioned Richardson iteration.

Due to Lemmas 3 and 5, the convergence rate of (14) does not depend on the meshsize and can be improved by applying a Krylov subspace method. When the difference between two successive iterations Ω_H^{n+1} and Ω_H^n satisfies a stopping criteria, then we can compute T_h^{n+1} by means of the first equation in (11). At this point, the moving conductor reaches its new position, and the algorithm (14) starts again.

The preconditioned Richardson iteration to obtain Ω_H^{n+1} is illustrated in Fig. 6. In each iteration step, we have to solve one Dirichlet problem on V_c associated with the Laplace operator, one Dirichlet problem on V_c associated with the curl operator, and one Dirichlet problem associated with the Laplace operator on V.

5. Numerical results

We apply the block Gauß–Seidel method (11) in two dimensions to the example shown in Fig. 7. The computational domain V is the square $(-0.1\text{ m}, 0.1\text{ m})^2$ containing a ferromagnet of permeability $\mu = 5 \cdot 10^{-4}$ H/m. Two coils generating the source field T_s are located on a part of the ferromagnet (shadowed part of Fig. 7, left). The conductor V_c of width 0.012 m and height 0.09 m moves with the constant velocity $v = -0.2\vec{e}_y$ m/s, its barycenter having the initial position $x_0 = (0, 0.01\text{ m})^t$. The conductivity σ of V_c is set to be 10^6 S/m, its magnetic permeability is the same as the one of the surrounding air, $\mu_0 = 4\pi 10^{-7}$ H/m. The used time step is $\delta t = 0.00625$ s.

The triangulation $\mathfrak{T}_H$ of the domain V consists of 1536 quadrilateral elements sharing 1616 nodes. The conductor V_c is discretized by means of 512 triangles yielding 808 edge element unknowns. We remark that the two meshes are completely independent. Moreover, the movement of the conductor is performed without involving any remeshing procedure. The application of the matrix $K_{0;V}^{-1}$ and the application of the Schur complement $\mathscr{S}_K$ is carried out in terms of a multigrid method. To apply $\mathscr{S}_A$, we use a direct solver. We note that $\mathscr{S}_A$ is independent of the time step. Thus it is sufficient to carry out a LU-decomposition of $\mathscr{S}_A$ only once. The presented algorithm consists of two nested iterative schemes. An implicit Euler scheme is used for the outer iteration with zero initial condition. The inner iteration is the preconditioned Richardson method given in (14).

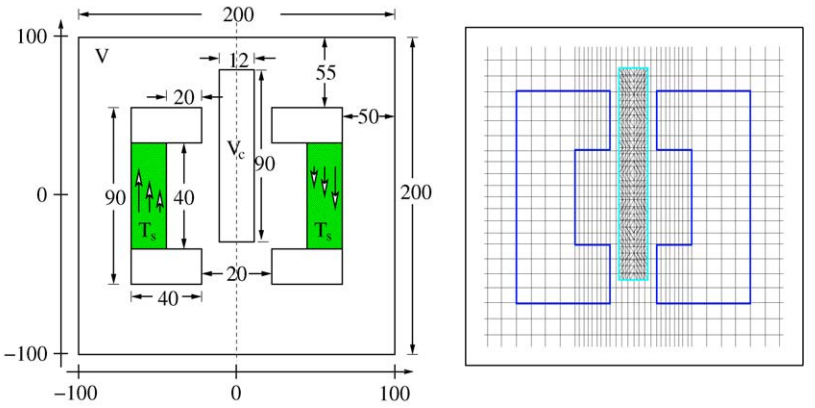

Fig. 7. Left: conductor V_c moving through the magnetic field induced by T_s. Here, dimensions are given in millimeters. Right: overlapping nonmatching grids (zoom).

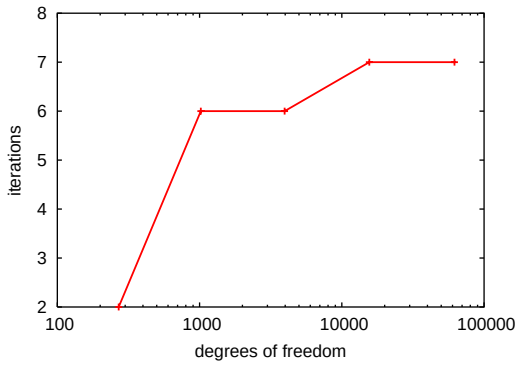

Fig. 8. Time step 8. Number of iteration steps with respect to the number of unknowns.

We use $\|\Omega_H^{n+1} - \Omega_H^n\|/\|\Omega_H^n\| < 10^{-4}$ as stopping criteria for our inner iteration scheme. For the considered example, the number of iterations is between 5 and 11 for all time steps. Fig. 8 illustrates the preconditioned Richardson iteration for a fixed time step. To support the theoretical result of Lemma 3, we consider different meshsizes and show the number of required iteration steps versus the number of unknowns. We observe convergence rates which are independent of the meshsizes.

Figs. 9 and 10 show the distribution of the magnetic field outside and inside the conductor V_c corresponding to two different positions of the moving part V_c. The distribution of the induced field in the conductor is in agreement with that predicted by the Lenz law, i.e., the induced currents create a field which contrasts the one generated by the sources in order to give a zero total magnetic field in V_c.

In Fig. 11, the components of the magnetic field in horizontal direction are plotted along the vertical axis of symmetry, which is indicated by the dashed line in Fig. 7, left. The inducing component $-\partial_x\Omega$ generates a reaction field T_x in V_c trying to compensate the first one. Thus these two components have opposite signs. After the first time step, the resulting total field $(T - \nabla\Omega)_x$

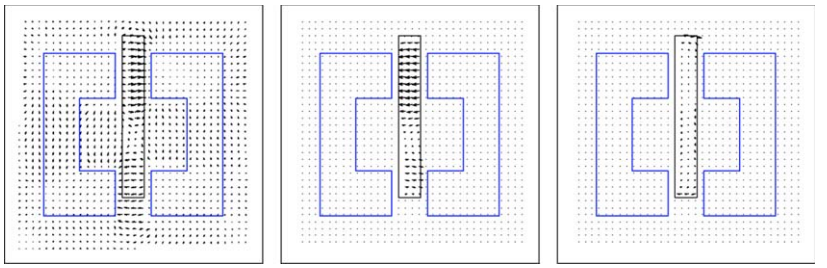

Fig. 9. Time step 1. Left: generated field $-\nabla\Omega$ in V between the poles. Middle: induced vector potential T on V_c. Right: magnetic field $H = T - \nabla\Omega$ on V_c.

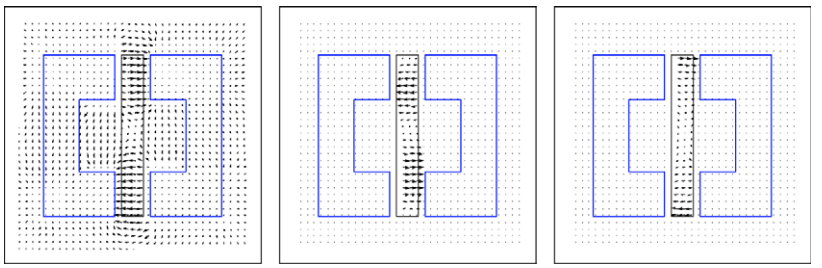

Fig. 10. Time step 8. Left: generated field $-\nabla\Omega$ in V between the poles. Middle: induced vector potential T on V_c. Right: magnetic field $H = T - \nabla\Omega$ on V_c.

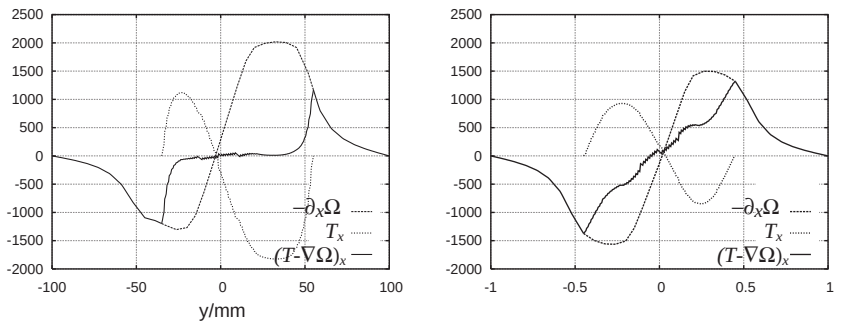

Fig. 11. Field intensity in horizontal direction along the vertical axis of symmetry: time step 1 (left), time step 8 (right).

inside the conductor is almost completely suppressed because of the instantaneous penetration by the inducing field, as shown in the left picture of Fig. 11. As the conductor moves along, this effect becomes less intense. Moreover, even when the barycenter of V_c is exactly at the origin of the system, the field distribution in V_c is not symmetric with respect to the horizontal axis, as illustrated in the right picture of Fig. 11. This is due to the motion of the conductor towards the bottom.

Further developments of the proposed method are in progress to state its flexibility, potentialities and to extend the implementation to three-dimensions. We remark that the method is well suited to simulate coupled magneto-mechanical systems, [5]. It is of special interest for the numerical simula-

tion of an electromagnetic brake. In that case, the forces due to the magnetic field contribute to the free structure motion. The resulting variation in the structure configuration modifies the distribution of the magnetic field and thus of the induced forces.

References

[1] R. Albanese, G. Rubinacci, Formulation of the eddy-current problem, IEE Proc. A 137 (1990) 16–22.
[2] C. Bernardi, Y. Maday, A. Patera, A new nonconforming approach to domain decomposition: the mortar element method, in: H. Brezis, J. Lions (Eds.), Nonlinear Partial Differential Equations and Their Applications, Pitman, London, 1994, pp. 13–51.
[3] A. Bossavit, Computational Electromagnetism: Variational Formulations, Complementarity, Edge Elements, Academic Press, New York, 1998.
[4] C.R.I. Emson, C.P. Riley, D.A. Walsh, K. Ueda, T. Kumano, Modelling eddy currents induced in rotating systems, IEEE Trans. Magn. 34 (1998) 2593–2596.
[5] B. Flemisch, Y. Maday, F. Rapetti, B.I. Wohlmuth, Scalar and vector potentials' coupling on nonmatching grids for the simulation of an electromagnetic brake, Compumag 2003 Proceedings, Saratoga Spring, to appear.
[6] E. Heikkola, Y.A. Kuznetsov, P. Neittaanmäki, J. Toivanen, Fictitious domain methods for the numerical solution of two-dimensional scattering problems, J. Comput. Phys. 145 (1998) 89–109.
[7] Y. Maday, F. Rapetti, B.I. Wohlmuth, Coupling between scalar and vector potentials by the mortar element method, C. R. Acad. Sci. Paris, Ser. I 334 (2002) 933–938.
[8] Y. Maday, F. Rapetti, B.I. Wohlmuth, Mortar element coupling between global scalar and local vector potentials to solve eddy current problems, in: F. Brezzi, A. Buffa, S. Corsaro, A. Murli (Eds.), Numerical Mathematics and Advanced Applications, Enumath 2001 Proceedings, Springer, Italy, 2003, pp. 847–865.
[9] J.-C. Nédélec, Mixed finite elements in $\mathbb{R}^3$, Numer. Math. 35 (1980) 315–341.
[10] J.-C. Nédélec, Acoustic and Electromagnetic Equations: Integral Representation for Harmonic Problems, Springer, New York, 2001.
[11] Y. Saad, Iterative Methods for Sparse Linear Systems, PWS Publishing Company, Boston, MA, 1996.
[12] B.I. Wohlmuth, Discretization methods and iterative solvers based on domain decomposition, Lecture Notes in Computational Sciences and Engineering, Vol. 17, Springer, Heidelberg, 2001.